

Synthesis of $\text{Al}(\text{N}_3)_3$ and the Deposition of AlN Thin Films

C. J. Linnen, D. E. Macks, and R. D. Coombe*

Department of Chemistry and Biochemistry, University of Denver, Denver, Colorado 80208

Received: August 21, 1996; In Final Form: November 19, 1996[⊗]

$\text{Al}(\text{N}_3)_3$ is produced by the stoichiometric reaction between $\text{Al}(\text{CH}_3)_3$ and excess HN_3 at room temperature. The reaction is thought to proceed by the addition of HN_3 to $\text{Al}(\text{CH}_3)_3$ followed by elimination of CH_4 , repeated three times to produce the fully azidified $\text{Al}(\text{N}_3)_3$. The product $\text{Al}(\text{N}_3)_3$ is nonvolatile and condenses as a film on the walls of the reaction vessel. The reaction products were observed in the gas phase and in low-temperature argon matrices by FTIR spectroscopy. Ab initio methods were used to compute the geometry and frequencies of $\text{Al}(\text{N}_3)_3$, and the results are in good agreement with experimental data. The films produced upon condensation of $\text{Al}(\text{N}_3)_3$ contain the $\text{Al}-\text{N}_2$ complex and AlN as well as the azide. Heating the films to 400 K removes the azide and the $\text{Al}-\text{N}_2$, leaving AlN. This method may be useful as a low-temperature route to the synthesis of AlN thin films.

I. Introduction

Aluminum nitride thin films have become increasingly important to the field of optoelectronics. Because of the piezoelectric properties, wide bandgap, and high thermal and chemical stability of this material, AlN films have been suggested for applications ranging from dielectric insulators¹ to surface acoustic wave devices² to second harmonic generation.³ Methods for synthesis of these films have typically involved inconvenient reagents in extreme conditions, however, with precursor dissociation temperatures on the order of 900 K. Because of the nature of VLSI and ULSI microcircuit technology, high temperatures can be a considerable detriment in device fabrication. As a result, an established trend in AlN thin film synthesis has been toward lower deposition temperatures, achieved by many different techniques including ion beam sputtering,^{4–6} molecular beam epitaxy,^{7,8} laser ablation,⁹ and a host of chemical vapor deposition (CVD) methods.

MOCVD methods for the deposition of AlN were introduced in 1971 by Manesvit and co-workers,¹⁰ who generated AlN by the reaction of $\text{Al}(\text{CH}_3)_3$ with NH_3 at high temperature. This reaction produces AlN and CH_4 at 1500 K. It is thought to proceed via the formation of an $\text{Al}(\text{CH}_3)_3:\text{NH}_3$ adduct, with the high temperature needed for breakage of the strong N–H bonds. Lower deposition temperatures (1000 K) were achieved by Gaskill and co-workers,¹¹ by replacing the NH_3 reagent with the considerably more reactive species hydrazine. Interrante and co-workers¹² investigated the use of organometallic amides as precursors to AlN films. The approach was to synthesize and dissociate species similar to the intermediates in the $\text{Al}(\text{CH}_3)_3 + \text{NH}_3$ reaction, the most volatile of which was found to be the $[(\text{CH}_3)_2\text{Al}(\text{NH}_2)]_3$ trimer. This species had the additional advantage of fixing the Al:N stoichiometry at 1:1. In 1989, Boyd and co-workers¹³ reported the deposition of AlN by the dissociation of metal-organic aluminum azides, species which are still more energetic. Using this approach, deposition temperatures as low as 700 K were achieved, but the syntheses of these compounds were complex and the films incorporated significant amounts of CH_4 and CN impurities. Very recently, deposition temperatures as low as 400 K were obtained through the use of organometallic amide complexes like $\text{Al}_2[\text{N}(\text{CH}_3)_2]_6$.¹⁴

Recent research in our laboratory¹⁵ has demonstrated a simple gas phase synthesis of fully azidified boron, $\text{B}(\text{N}_3)_3$, and its

subsequent thermal or photolytic dissociation to produce BN films. The synthesis was based on the stoichiometric reaction of BCl_3 with HN_3 . This reaction is thought to occur by initial formation of a $\text{BCl}_3:\text{HN}_3$ adduct, which can spontaneously eliminate HCl because of the relative weakness of the N–H bond in HN_3 . In this paper, we present the results of a study of an analogous gas phase reaction between $\text{Al}(\text{CH}_3)_3$ and HN_3 , which produces $\text{Al}(\text{N}_3)_3$ by the elimination of CH_4 . This compound and its adducts were originally prepared in 1954 by Wiberg and Michaud,¹⁶ who reacted gas phase HN_3 with a solution of aluminum hydride in ether at 77 K and then warmed the solution to room temperature. This method produced an extremely energetic association of loosely bound azide complexes which exhibited a marked tendency toward explosion. Perhaps because of this, compounds of fully azidified group III elements have received very little attention until the recent work in our laboratory. We present the synthesis of $\text{Al}(\text{N}_3)_3$, experimental and computational studies of its structure and vibrational characteristics in the gas phase and in low-temperature matrices, and a preliminary evaluation of the utility of this species as a precursor for AlN thin films.

II. Experimental Methods

Gaseous HN_3 was synthesized¹⁷ by reacting NaN_3 with an excess of stearic acid at 373 K. The middle fraction of the HN_3 generated was collected in a pyrex bulb and diluted 10-fold with He. The purity of the HN_3 in the mixture was examined by using FTIR spectroscopy, and its absolute concentration was determined from the well-known UV absorption at 268 nm.¹⁸ $\text{Al}(\text{CH}_3)_3$ was obtained from Alfa Products and was purified by successive freeze-thaw cycles at 273 K to remove the methane impurity.

Aluminum azides were generated by the spontaneous room temperature reaction between gaseous HN_3 and $\text{Al}(\text{CH}_3)_3$ vapor. The gases were handled in a stainless steel vacuum system, and pressures were measured with two MKS Baratron pressure transducers. It was necessary to passivate the system with $\text{Al}(\text{CH}_3)_3$ for at least 30 min prior to the experiments to obtain stable pressures of this compound in the system. The passivation process clearly produces CH_4 , features of which are observed to grow into the IR spectrum of the gas. This result suggests that methane is released as the aluminum binds to the metal surface, with methyl groups from the original $\text{Al}(\text{CH}_3)_3$

[⊗] Abstract published in *Advance ACS Abstracts*, February 15, 1997.

combining with H atoms displaced from the surface. Experiments showed that the passivation layer would react with HN₃ just as would gaseous Al(CH₃)₃. Consequently, it was difficult to distinguish aluminum azides created by wall reaction from those made in the vapor phase.

The reagents were mixed in an 11 cm cell fitted with either KCl or fused silica windows for FTIR or UV analysis, respectively. FTIR spectra were recorded with either a Nicolet 5DXC spectrometer or a Mattson Polaris spectrometer. UV-vis spectra were recorded with a Milton-Roy 3000 diode array spectrometer. Grazing incidence X-ray diffraction spectra of solid reaction products were recorded with a Siemens diffractometer.

Low-temperature matrix isolation experiments were performed by using an RMC Cryosystems LTS-22 closed cycle refrigerator. For these experiments, flowing streams of the reagents mixed with Ar were passed through a 5 L reaction vessel prior to being deposited onto the cold window of the apparatus. The flow rates of the reagents were measured with MKS mass flow meters.

III. Results and Discussion

1. Reaction of Al(CH₃)₃ with HN₃. By analogy with the reaction of BCl₃ with excess HN₃, Al(CH₃)₃ is expected to react stoichiometrically with HN₃ to generate Al(N₃)₃ and methane:



There is a significant difference between this system and the reaction of BCl₃ with HN₃, however, in that BCl₃ exists as a monomer at room temperature whereas Al(CH₃)₃ is primarily dimeric below 573 K.¹⁹ The formation of an Al(CH₃)₃:HN₃ adduct would require the breaking of the bridging methyl–aluminum bond in the dimer. Because of the additional energy needed, reaction 1 was expected to be much slower than the BCl₃ analog, if in fact it would occur at all at room temperature.

The initial experiments showed clearly that reaction was occurring, however. Figure 1a shows the IR spectrum of vapor phase Al(CH₃)₃ present in the reaction cell at 1.0 Torr, after thorough passivation. The spectra indicated that the compound was stable in the cell at this pressure for extended periods of time (hours), in the absence of air or atmospheric H₂O. Figure 1b shows the IR spectrum of 3.0 Torr of HN₃ (at 1:10 in He) in the cell, exhibiting the characteristic absorptions at 2150 and 1164 cm⁻¹ (stretches in the N₃ group) and 3324 cm⁻¹ (the N–H stretch). Figure 1c shows the IR spectrum obtained from a gas mixture in which 1.0 Torr of Al(CH₃)₃ was allowed to react with 3.0 Torr of HN₃ (1:10 in He) for a period of 8 min. The spectrum clearly shows the loss of the features corresponding to Al(CH₃)₃ and HN₃, and the evolution of CH₄ is evident from its characteristic absorptions at 3017 and 1306 cm⁻¹.²⁰ The spectrum of the reaction mixture still shows a feature near 2160 cm⁻¹, as in the HN₃ spectrum in Figure 1b, but the total absence of the HN₃ features at 1164 and 3340 cm⁻¹ indicates that this is *not* attributable to HN₃. Since virtually all azides have an absorption in the 2050–2150 cm⁻¹ region (corresponding to asymmetric stretching in the N₃ group), this result strongly suggests the formation of a new azide species.^{20,21}

The stoichiometry of reaction 1 was determined by analysis of IR spectra recorded for varying Al(CH₃)₃:HN₃ ratios, at a constant initial Al(CH₃)₃ pressure of 1.0 Torr. Spectra recorded for a variety of initial HN₃ pressures are shown in Figure 2. Qualitative scrutiny of the spectra clearly reveals the occurrence of the reaction. Perhaps most striking is the disappearance of the Al(CH₃)₃ spectrum, the growth of the methane features near

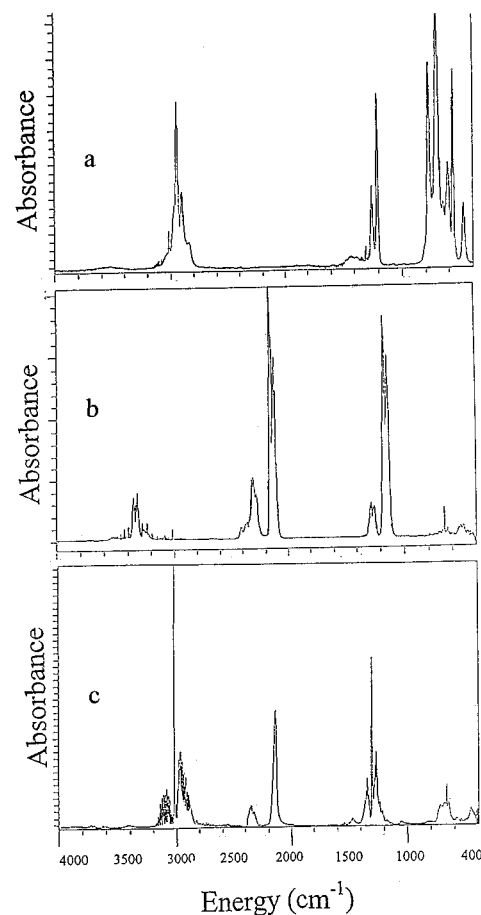


Figure 1. Gas phase mid-IR spectra of (a) 1 Torr of pure Al(CH₃)₃ after passivation of the cell for ~30 min, (b) 30 Torr of a 10% mixture of HN₃ in He, and (c) mixture of Al(CH₃)₃ with 3 equiv of HN₃ after allowing 8 min for reaction. A 10 cm long stainless steel cell fitted with KCl windows was used for all IR spectra.

3017 and 1306 cm⁻¹, and the appearance of the “new” N₃ stretching features at 2156 cm⁻¹. This feature is a single absorption peak, clearly different from the “doublet” appearance of the HN₃ feature in this region. Though significantly overlapped by methane and residual Al(CH₃)₃ features, new absorptions at 1250 and 741 cm⁻¹ grow in and appear to be correlated with the 2156 cm⁻¹ peak. At reaction stoichiometries above 2.5:1, as the reaction approaches completion (3:1), these new features at 2156, 1236, and 741 cm⁻¹ disappear almost completely. No other peaks appear to be growing in. Assuming that the features are attributable to aluminum azides (as discussed below), the disappearance might be attributed to the formation of Al(N₃)₃ as the stoichiometry approaches 3:1, as this species is expected to be nonvolatile at room temperature¹⁶ and should condense out on the vessel walls. This inference was supported by the observation of the formation of a deposit on the walls for the 3:1 stoichiometry.

A quantitative measure of the stoichiometry was obtained by measurement of the relative absorbance intensities of the reactant and product features as the mixing ratio increased. These data are shown in Figure 3 as a plot of absorbance vs the initial HN₃:Al(CH₃)₃ ratio. In the data shown, the HN₃ density was tracked by the N₃ stretching vibration of this molecule at 1164 cm⁻¹. The density of Al(CH₃)₃ was monitored by observing the features at 700 and 775 cm⁻¹. The data show that the Al(CH₃)₃ density decreases with added HN₃, falling to zero at a mixing ratio just below 3:1. Further, residual unreacted HN₃ appears in the spectrum at mixing ratios above 3:1. These data

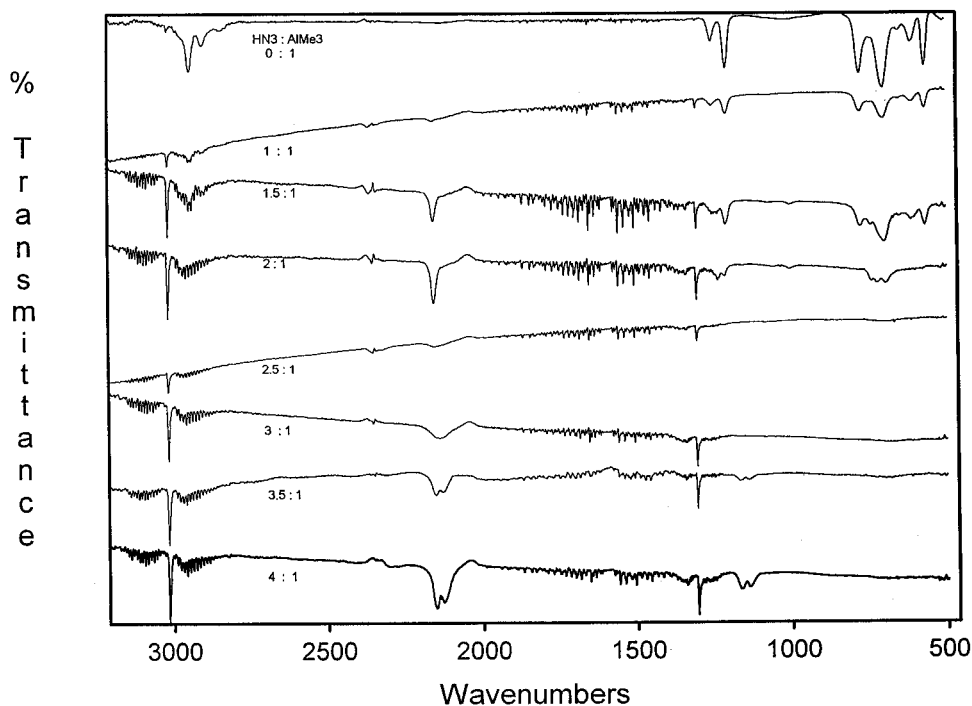


Figure 2. IR spectra obtained by varying the stoichiometric mixtures of HN_3 (1:10 in He) with 1 Torr of $\text{Al}(\text{CH}_3)_3$.

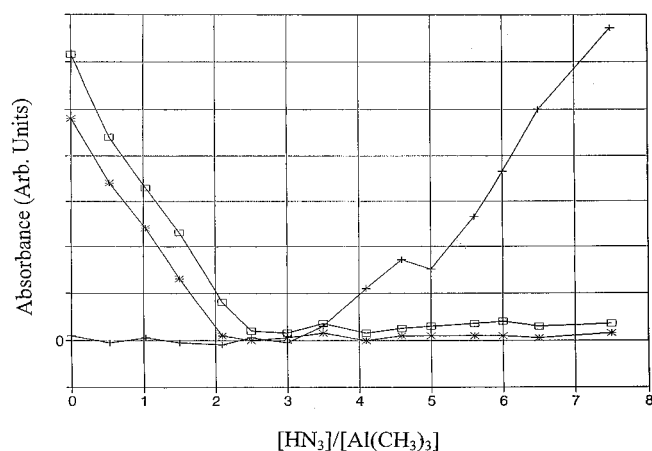


Figure 3. Plot of absorbance versus $\text{HN}_3:\text{Al}(\text{CH}_3)_3$ ratio. Varying pressures of a 10% mixture of HN_3 in He were added to 1 Torr of $\text{Al}(\text{CH}_3)_3$ to obtain the reagent ratios shown. (+) HN_3 peak at 1164 cm^{-1} , (*) $\text{Al}(\text{CH}_3)_3$ peak at 775 cm^{-1} , and (□) $\text{Al}(\text{CH}_3)_3$ peak at 700 cm^{-1} .

clearly indicate the 3:1 stoichiometry and suggest that reaction 1 proceeds to completion in our system.

Monitoring the stoichiometry via IR features of the products of the reaction was problematic. As noted, the aluminum azide features clearly grow into the spectrum with increasing HN_3 density but abruptly disappear near the 3:1 stoichiometric "end point", likely because of condensation of the fully azidified $\text{Al}(\text{N}_3)_3$. The methane product was easily tracked and clearly grew in as expected for mixing ratios below 3:1, but though the absorbance flattened somewhat at higher ratios, its growth continued. This may be attributable to HN_3 reaction with $\text{Al}(\text{CH}_3)_3$ in the passivation layer on the vessel walls, with the product aluminum azide remaining on the wall but the methane released to the gas phase. Hence the methane absorbance did not show a sharp end point at the 3:1 gas phase mixing ratio. Nonetheless, the end point is clear from the data in Figure 3. It is interesting to consider the fact that complete reaction with the $\text{Al}(\text{CH}_3)_3$ dimers initially present would give rise to a 4:1 stoichiometry (assuming that the dimers retained the two

bridging methyl groups) or that a 6:1 stoichiometry would result if HN_3 reacts only with monomers (as expected) and the gas phase dimer \leftrightarrow monomer equilibrium slowly responded to replenish the monomers. Clearly, neither of these possibilities is in accord with the data. It seems likely, particularly in view of the slow rate of the reaction (see below), that reaction at the walls is important. For example, HN_3 might react with the dimer at the walls, releasing a gaseous $\text{AlN}_3(\text{CH}_3)_2$ moiety (capable of reacting with two more HN_3 molecules), leaving the residual $\text{Al}(\text{CH}_3)_3$ monomer strongly bound to the metal wall. Such wall-bound monomers would react only very slowly, giving rise to the slow evolution of CH_4 observed for HN_3 densities in excess of the 3:1 stoichiometry.

In the course of recording the spectra shown in Figure 2, it was indeed apparent that the reaction between $\text{Al}(\text{CH}_3)_3$ and HN_3 is very much slower than the analogous $\text{BCl}_3 + \text{HN}_3$ reaction studied earlier. In the latter case, the reaction appeared to be immediate; i.e., the reactants were consumed and products fully formed in the time necessary to record the spectra. For the reaction with $\text{Al}(\text{CH}_3)_3$, complete reaction required on the order of 10 min after mixing, for normal conditions (1.0 Torr of $\text{Al}(\text{CH}_3)_3$ at 298 K). In an effort to quantify these observations, spectra were recorded at fixed times after mixing, and the data were converted to time profiles of the reactant and product species. Figure 4 shows such time profiles recorded for HN_3 and CH_4 at a 3:1 reactant mixing ratio. The symmetry between the loss of HN_3 and the growth of CH_4 is apparent. Note that the CH_4 density continues its slow growth at long times, as described above. An effective rate constant can be obtained from fitting data such as these to rate expressions which assume second-order kinetics. Good fits are obtained, and these indicate an effective reaction rate constant on the order of $10^{-20}\text{ cm}^3\text{ s}^{-1}$. The very small magnitude of this effective rate constant certainly underscores the notion that the walls are important in the reaction mechanism. Calculations of the energetics of the $\text{BCl}_3 + \text{HN}_3$ reaction suggested that the first step in the reaction sequence (formation of Cl_2BN_3) was likely to be rate limiting. While this may also be true for the reaction with $\text{Al}(\text{CH}_3)_3$, the very slow rate of this process certainly

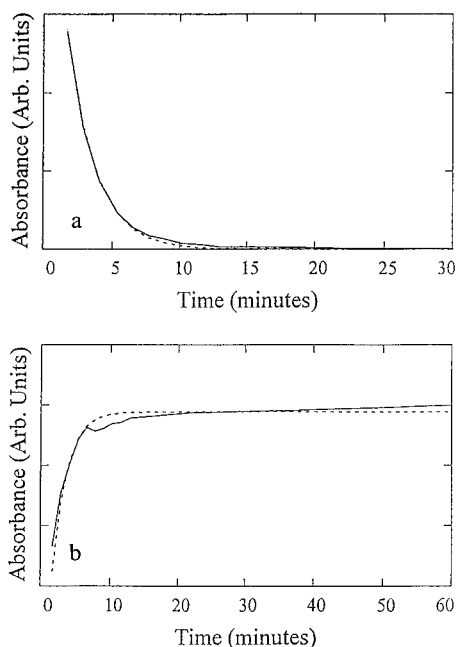


Figure 4. Time profile showing (a) the decay of HN_3 and (b) the associated CH_4 growth.

TABLE 1: Calculated Geometry Parameters for $\text{Al}(\text{N}_3)_3$

parameter	RHF/6-31G(d)	RMP2/6-31 G(d)
$\text{Al}-\text{N}_\alpha$ (Å)	1.768	1.787
$\text{N}_\alpha-\text{N}_\beta$ (Å)	1.215	1.229
$\text{N}_\beta-\text{N}_\gamma$ (Å)	1.099	1.175
$\angle \text{X}_1^a-\text{Al}-\text{N}_\alpha$ (deg)	90.0	90.0
$\angle \text{Al}-\text{N}_\alpha-\text{N}_\beta$ (deg)	134.1	133.4
$\angle \text{X}_1^a-\text{Al}-\text{N}_\alpha-\text{N}_\beta$ (deg)	90.1	90.1
$\angle \text{X}_2^b-\text{N}_\beta-\text{N}_\alpha$ (deg)	90.1	90.3
$\angle \text{Al}-\text{N}_\alpha-\text{N}_\beta-\text{X}_2^b$ (deg)	86.7	84.4
$\angle \text{X}_3^b-\text{N}_\beta-\text{N}_\alpha$ (deg)	88.2	87.4
$\angle \text{N}_\alpha-\text{Al}-\text{N}_\alpha$ (deg)	120	120

^a X_1 : dummy atom placed on Al. ^b X_2, X_3 : dummy atoms placed on N_β .

implies that the rate is somehow limited by the dimer \leftrightarrow monomer equilibrium.²² The system may be further complicated by the documented tendency of partially azidified intermediates (e.g., $(\text{CH}_3)_2\text{AlN}_3$) to trimerize.¹³ It seems unlikely, however, that trimerization would compete with reaction given the greater densities of HN_3 always present. Indeed, the spectra shown in Figures 1 and 2 indicate the complete removal of methyl-aluminum species.

2. Calculations of the Structure and Frequencies of $\text{Al}(\text{N}_3)_3$. Ab initio calculations of the structure and vibrational frequencies of monomeric $\text{Al}(\text{N}_3)_3$ were performed in an effort to more clearly characterize the IR spectra described above. The calculations were performed by using the GAUSSIAN 92 family of programs²³ at the HF/6-31G(d) and MP2/6-31G(d) levels of theory. In each case, partial geometry optimizations were performed which assumed the equivalent geometry within each of the N_3 groups. For similar calculations done on $\text{B}(\text{N}_3)_3$, this assumption produced a geometry for which calculated frequencies agreed very well with experimental IR spectra. The results of the geometry optimizations for $\text{Al}(\text{N}_3)_3$ are shown in Table 1. The RHF and MP2 calculations show considerable consistency. The value of 133° calculated at the MP2 level for the $\text{Al}-\text{N}_\alpha-\text{N}_\beta$ bond angle is substantially larger than the analogous angle calculated for $\text{B}(\text{N}_3)_3$ (120°). This may indicate greater inclusion of s atomic orbital character into the bonding orbitals on N_α . In another sense, it may reflect the lesser formal covalency of the Al-N bond (53%) with respect to the B-N

TABLE 2: Calculated Frequencies (cm^{-1}) for $\text{Al}(\text{N}_3)_3$

level of theory	$\nu(\text{AlN}_3)$ (rel int)	$\delta(\text{N}_3)$ (rel int)	$\nu_{\text{sym}}(\text{N}_3)$ (rel int)	$\nu_{\text{asym}}(\text{N}_3)$ (rel int)
RMP/6-31 G(d)	568 (21)	737 (251)	1366 (210)	2192 (1011)
obsd: gas phase		741	1236	2156
obsd: matrix studies		730	1360	2160

bond (74% covalent); fully ionic azides are generally linear. The $\text{N}_\alpha-\text{N}_\beta$ and $\text{N}_\beta-\text{N}_\gamma$ bond lengths as well as the $\text{N}_\alpha-\text{N}_\beta-\text{N}_\gamma$ angle are very similar to those calculated for $\text{B}(\text{N}_3)_3$. The value of 1.79 Å for the $\text{Al}-\text{N}_\alpha$ bond length is considerably longer than that of the $\text{B}-\text{N}_\alpha$ bond (1.44 Å) as expected, but is somewhat shorter than Al-N bonds in other compounds (approximately 1.9 Å). This shorter $\text{Al}-\text{N}_\alpha$ bond length may reflect back-donation of the azide π electron density into low-lying unoccupied d-type orbitals on the Al atom.

Frequency calculations were performed for the optimized geometry at the MP2/6-31G(d) level of theory, and the results are shown in Table 2. Of the 24 normal modes of $\text{Al}(\text{N}_3)_3$, only four were found to have appreciable IR intensity in the mid-IR region. As shown in the table, the calculated results are in reasonable agreement with experiment. The most intense peak is predicted to lie at 2192 cm^{-1} , only 36 cm^{-1} to the blue of the experimental result. The calculation predicts less intense lower frequency features at 1366 and 737 cm^{-1} . These too agree with experimental frequencies, although these features are obscured by $\text{Al}(\text{CH}_3)_3$ and CH_4 absorptions in our experimental spectra. We note also that perfect agreement is not expected since the experimental spectra may well contain features corresponding to partially azidified molecules (as $\text{Al}(\text{N}_3)_3$ is expected to be condensed on the vessel walls). Further clarification was sought in the matrix isolation experiments described below.

Using the minimum energy calculated for the optimized $\text{Al}(\text{N}_3)_3$ geometry, and calculations of the energies of $\text{Al}(\text{P})$ and $\text{N}_2(^1\Sigma_g^+)$ done at the same level of theory, the heat of formation of $\text{Al}(\text{N}_3)_3$ (corrected for zero-point energies) was calculated to be $\Delta H_{f,298} = 84.7 \text{ kcal/mol}$. While this value is substantially larger than that calculated for $\text{B}(\text{N}_3)_3$ (21.2 kcal/mol),¹⁵ the stability of methane relative to HCl leads to an overall exothermicity for reaction 1 of -164 kcal/mol , quite similar to the value calculated for the analogous formation of $\text{B}(\text{N}_3)_3$ from BCl_3 and HN_3 . Using average bond energies, the initial $\text{Al}(\text{CH}_3)_3 + \text{HN}_3$ reaction is calculated to be exothermic by 29 kcal/mol , adding further support to the notion that the rate is controlled by the dimer/monomer equilibrium.

3. Low-Temperature Matrix Isolation Studies. Matrix isolation experiments were performed in an effort to better resolve features in the IR spectra corresponding to reactants and different possible products. In particular, it was hoped that the matrix experiments would allow better resolution of the aluminum azide features from HN_3 features in the 2150 cm^{-1} region and resolution of aluminum azide from methane in the low-frequency region.

Following passivation of the system, $\text{Al}(\text{CH}_3)_3$ and argon (at a 100-fold excess of argon) were flowed through the system and onto the cold window until the characteristic IR features of the $\text{Al}(\text{CH}_3)_3$ were clearly visible and the growth of methane features (a passivation product) reached a minimum. A flow of HN_3 was then added to achieve the 3:1 stoichiometric mixing ratio. For typical conditions, the residence time in the reaction bulb (i.e., prior to deposition of the mixture) was on the order of 10 min, such that complete reaction was assured. The system was very responsive to the HN_3 flow rate, and the reaction stoichiometry was easily manipulated. For a 3:1 flow ratio, no excess HN_3 was evident in the IR spectrum of the matrix.

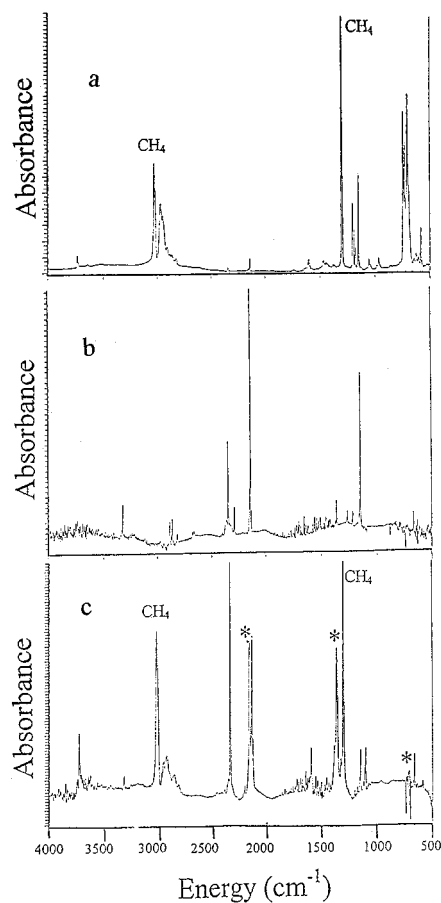


Figure 5. IR spectra of (a) $\text{Al}(\text{CH}_3)_3$ (1:100 in Ar), (b) HN_3 (1:100 in Ar), and (c) mixture of $\text{Al}(\text{CH}_3)_3$ with HN_3 at a 3:1 stoichiometric flow rate (see section III.3) isolated in a ~ 10 K argon matrix.

Raising the HN_3 flow rate by only 3% clearly introduced HN_3 features into the spectrum.

Parts a and b of Figure 5 show spectra of matrices containing the reagents $\text{Al}(\text{CH}_3)_3$ and HN_3 , respectively. Both are in very good agreement with similar spectra presented in the literature.²⁴ The extensive passivation requirement for the $\text{Al}(\text{CH}_3)_3$ matrix is reflected in the presence of intense CH_4 features at 1305 and 3024 cm^{-1} . The HN_3 spectrum (Figure 5b) exhibits features corresponding to trapped CO_2 , a byproduct of the HN_3 synthesis. Figure 5c shows the spectrum of a matrix made by deposition of the 3:1 stoichiometric mixture as described above. While it shows evidence of unreacted $\text{Al}(\text{CH}_3)_3$ and HN_3 (artifacts of the deposition method: the $\text{Al}(\text{CH}_3)_3$ was deposited during passivation, and the HN_3 appeared only when the mixing ratio was adjusted to be slightly in excess of 3:1), it also clearly shows features corresponding to the products CH_4 and aluminum azide, the latter marked with an asterisk. The high-frequency N_3 stretch in the aluminum azide (2160 cm^{-1}) is clearly separated from the analogous feature in HN_3 (2137 cm^{-1}). Further, the lower frequency features at 1361 and 730 cm^{-1} are easily resolved.

These data lend credence to the assignments from the gas phase spectra described above. Further, from the sensitivity to the stoichiometry and the fact that the matrix environment does not distinguish between volatile and nonvolatile products, the trapped species is expected to be the fully azidified $\text{Al}(\text{N}_3)_3$. Indeed, the observed frequencies are in better agreement with those calculated for this molecule (as above) than are the gas phase results.

4. Deposition and Dissociation of $\text{Al}(\text{N}_3)_3$. After several successive gas mixtures were allowed to react within the IR

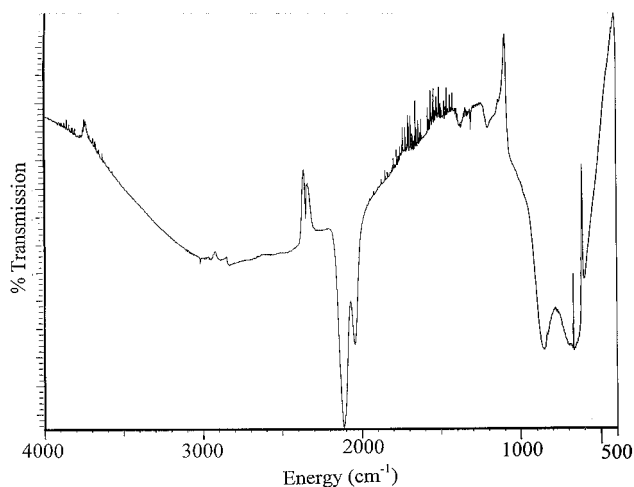


Figure 6. Difference spectrum obtained by subtraction of a single-beam scan taken of clean KCl windows from a single-beam scan of the same windows with film residue created from the reaction of HN_3 with $\text{Al}(\text{CH}_3)_3$ at 3:1 stoichiometry.

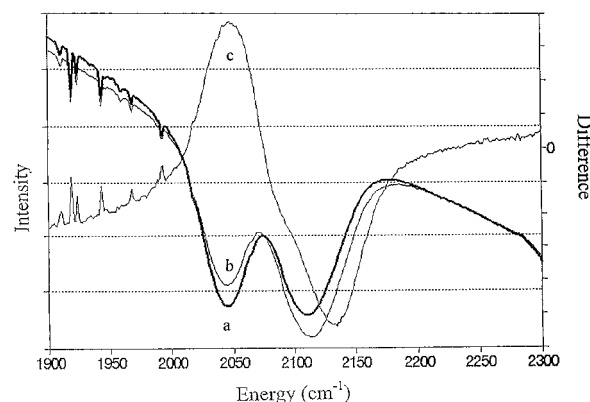


Figure 7. IR spectra of (a) 1900–2300 cm^{-1} region of the spectrum shown in Figure 6, (b) 1900–2300 cm^{-1} region of the film represented by Figure 6 after exposure to heat (~ 100 °C) for 20 min, and (c) difference spectrum obtained by subtraction of (a) from (b).

cell, a persistent absorbance was apparent in the background spectrum (i.e., in the spectrum of the evacuated cell). Figure 6 shows a spectrum of this absorbance, obtained by subtraction of the spectrum of a clean KCl window from the spectrum of the cell after contact with several reaction mixtures. A broad absorbance in the 500–1000 cm^{-1} region, in good agreement with well-known AlN phonon modes,²⁵ is clearly evident. In addition, two sharper features are seen at 2043 and 2111 cm^{-1} . These features might be attributable to N_3 stretching vibrations of $\text{Al}(\text{N}_3)_3$ in the film (as noted above, this should be a nonvolatile reaction product) or perhaps to the $\text{Al}-\text{N}_2$ complex in the film formed by dissociation of the azide in the generation of the AlN . Mazur and Cleary⁵ have observed such complexes in the IR spectra of AlN films deposited by ion beam sputtering. To test these hypotheses, the evacuated cell was gently heated with the thought that heating would lead to further decomposition of the azide and generation of more N_2 . The cell was heated to a maximum temperature of 373 K for 30 min. Figure 7 shows the resulting IR spectra in the 1900–2300 cm^{-1} range. The difference spectrum (obtained by subtraction of the spectra before and after heating) clearly shows that heating leads to diminished intensity in the 2043 cm^{-1} band and increased intensity in the 2111 cm^{-1} band. On the basis of these data, we tentatively assign the 2043 cm^{-1} band to the N_3 stretching vibration in $\text{Al}(\text{N}_3)_3$ and the 2111 cm^{-1} band to the $\text{Al}-\text{N}_2$ complex in the film.

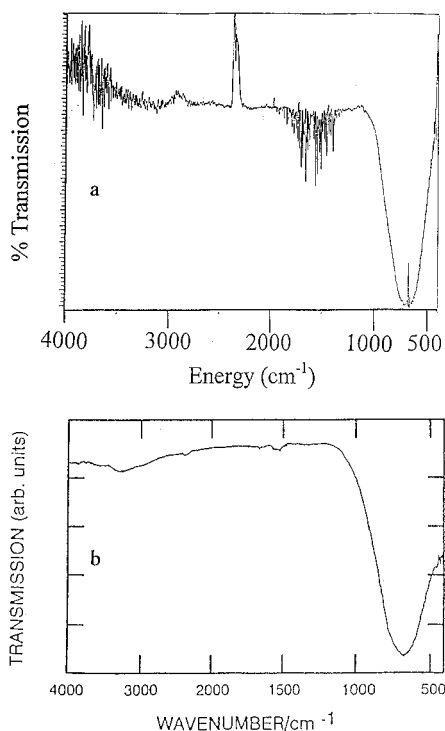


Figure 8. (a) Spectrum of film represented in Figure 6 after prolonged (~ 1 h) exposure to heat (~ 100 °C). (b) Spectrum of AlN thin film created by laser ablation. Reprinted with permission from ref 9. Copyright 1992 American Institute of Physics.

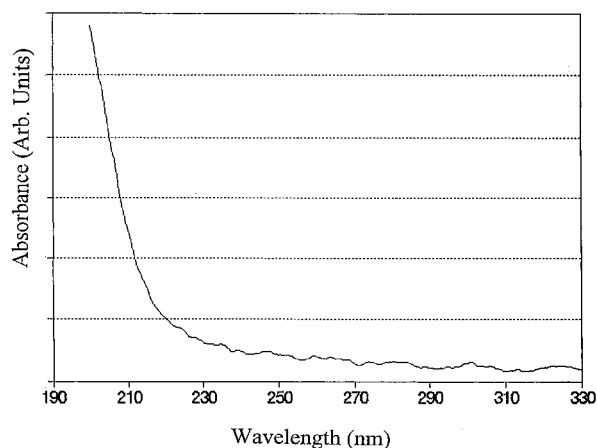


Figure 9. UV absorption spectrum of AlN film prepared by thermal dissociation of $\text{Al}(\text{N}_3)_3$ created by mixture of 1 Torr of $\text{Al}(\text{CH}_3)_3$ with 30 Torr of 1:10 HN_3 in He.

On further heating of the evacuated cell, to a maximum temperature of 400 K for 60 min, both the 2143 and 2111 cm^{-1} features disappeared completely. The broad AlN absorbance below 1000 cm^{-1} remained, however, as shown in Figure 8a. This spectrum is nearly identical to that reported in the literature for amorphous AlN produced by laser ablation, as shown in Figure 8b.⁹

Figure 9 shows the UV absorption spectrum of an AlN film produced by reaction of 3:1 gas mixtures in a cell with fused silica windows. The cell was not heated and should therefore contain both AlN and $\text{Al}(\text{N}_3)_3$. The spectrum shows little or no absorbance at wavelengths above 230 nm, but the absorbance rises steeply below 210 nm. Gas phase $\text{B}(\text{N}_3)_3$ exhibits a strong absorbance,¹⁵ believed to be the $n \rightarrow \pi^*$ transition in the azide moiety, at 230 nm. The lack of such an absorbance feature in the spectrum of Figure 9 reflects the considerably different bonding characteristics involved in $\text{Al}(\text{N}_3)_3$ with respect to the

boron analog. We note again that this is also reflected in the much larger $\text{Al}-\text{N}_\alpha-\text{N}_\beta$ bond angle as given by calculation. In recording spectra such as that shown in Figure 9, great care was taken to ensure that background absorptions associated with the spectrometer or the windows were adequately subtracted. The absorption onset is in very good agreement with the spectra of AlN films reported in the literature and corresponds well with the known bandgap of this material at 6.2 eV.⁸

A number of experiments were performed in an effort to obtain X-ray diffraction spectra of the AlN films. Powder samples were prepared by scraping the film from the interior surfaces of the reaction cell. These experiments were inconclusive, however, as the X-ray spectra obtained showed small features attributable to AlN but were dominated by features attributable to alumina (Al_2O_3) and NH_3 . It is well-known that these products arise from reaction of fresh AlN with atmospheric water:²⁶



The films were exposed to the atmosphere in the course of measurement of the diffraction spectra. Indeed, upon exposure to moist air, the IR spectra of the films (as in Figures 7 and 8) changed to include a broad high-frequency feature just above 3000 cm^{-1} , characteristic of ammonia in the film, and features near 950 cm^{-1} attributable to Al–O stretching vibrations.²⁷

IV. Summary and Conclusions

The data presented have shown that aluminum azides may be prepared by the spontaneous room temperature reaction between $\text{Al}(\text{CH}_3)_3$ and HN_3 . The reaction is quite slow at 298 K, likely because $\text{Al}(\text{CH}_3)_3$ exists primarily as a dimer at this temperature. From studies of the stoichiometry of the reaction, the infrared spectra of the reaction products, and comparison of these data with computed spectra, it is apparent that in the presence of sufficient HN_3 the reaction proceeds to the fully azidified $\text{Al}(\text{N}_3)_3$. This molecule is not volatile at 298 K, however, and condenses as a film on the walls of the reaction cell.

In the course of its preparation and condensation at room temperature, some of the $\text{Al}(\text{N}_3)_3$ decomposes to form Al– N_2 complexes and AlN. These species are observed in IR spectra of the films produced by the reaction, along with undissociated $\text{Al}(\text{N}_3)_3$. Gentle heating removes the azide and the Al– N_2 complex from the film, leaving what appears to be amorphous AlN. These results suggest that good quality AlN films might be generated by continuous flow of the stoichiometric 3:1 $\text{Al}(\text{CH}_3)_3:\text{HN}_3$ mixture over a substrate heated to perhaps 400 K. The gentle heating would serve two purposes: to accelerate the reaction and to drive off $\text{Al}(\text{N}_3)_3$ and free N_2 from the film. We are currently testing these thoughts by exploring the temperature dependence of the reaction.

Acknowledgment. This work was supported by the U.S. Air Force Office of Scientific Research under Grant F49620-93-1-0631 and by the National Science Foundation under Grant CHE-9300383. Special thanks go to Dr. Julanna Gilbert at the University of Denver for her assistance in low-temperature matrix isolation experiments.

References and Notes

- (1) Baier, H.-U.; Monch, W. *J. Appl. Phys.* **1990**, *68*, 586.
- (2) Pearce, L. G.; Gunshor, R. L.; Pierret, R. F. *Appl. Phys. Lett.* **1981**, *39*, 878.
- (3) Lundquist, P. M.; Lin, W. P.; Xu, Z. Y.; Wong, G. K.; Rippert, E. D.; Helfrich J. Al; Ketterson, J. B. *Appl. Phys. Lett.* **1994**, *65*, 1085.

- (4) Kubota, K.; Kobayashi, Y.; Fujimoto, K. *J. Appl. Phys.* **1989**, *66*, 2984.
- (5) Mazur, U.; Cleary, A. C. *J. Phys. Chem.* **1990**, *94*, 189. Wang, X. D.; Hipps, K. W.; Mazur, U. *J. Chem. Phys.* **1992**, *96*, 8485.
- (6) Zarwasch, R.; Rille, E.; Pulker, H. K. *J. Appl. Phys.* **1992**, *71*, 5275.
- (7) Yoshida, S.; Misawa, S.; Fujii, Y.; Takada, S.; Hayakawa, H.; Fonda, S.; Itoh, A. *J. Vac. Sci. Technol.* **1970**, *16*, 990.
- (8) Yim, W. M.; Strofko, E. J.; Zanzucchi, P. J.; Pankove, J. I.; Etnenberg, M.; Gilbert, S. L. *J. Appl. Phys.* **1973**, *44*, 292.
- (9) Seki, K.; Xu, X.; Okabe, H.; Frye, J.; Halpern, J. *J. Appl. Phys. Lett.* **1992**, *60*, 2234.
- (10) Manesevit, H. M.; Erdmann, F. M.; Simpson, W. I. *J. Electrochem. Soc.* **1971**, *118*, 1864.
- (11) Gaskill, D. K.; Bottka, N.; Lin, M. C. *J. Cryst. Growth* **1986**, *77*, 418.
- (12) Interrante, L. V.; Carpenter, Jr., L.; Whitmarsh, C.; Lee, W.; Garbavkas, M.; Alsck, G. A. *Mater. Res. Soc. Symp. Proc.* **1986**, *77*, 418.
- (13) Boyd, D. C.; Haasch, R. T.; Mantell, D. R.; Schulze, R. K.; Evans, J. F.; Gladfelter, W. L. *Chem. Mater.* **1989**, *1*, 119.
- (14) Hoffman, D. M.; Rangarajan, S. P.; Satish, D. A.; Economou, D. J.; Liu, J.-R.; Zheng, Z.; Chu, W.-K. *J. Vac. Sci. Technol. A* **1996**, *14*, 306.
- (15) Mulinax, R. L.; Okin, G. S.; Coombe, R. D. *J. Phys. Chem.* **1995**, *99*, 6294.
- (16) Wiberg, E.; Michaud, H. *Z. Naturforsch., Teil B* **1954**, *9*, 495.
- (17) Schlie, L. A.; Wright, M. W. *J. Chem. Phys.* **1990**, *92*, 394.
- (18) McDonald, J. R.; Rabalais, J. W.; McGlynn, S. P. *J. Chem. Phys.* **1970**, *85*, 290.
- (19) Kvisle, S.; Rytter, E. *J. Mol. Struct.* **1984**, *117*, 51.
- (20) Nakamoto, K. *Infrared and Raman Spectra of Inorganic and Coordination Compounds*; John Wiley & Sons: New York, 1986.
- (21) Patai, S. *The Chemistry of the Azido Group*; John Wiley & Sons: New York, 1971; Chapter 1.
- (22) Smith, M. B. *J. Organomet. Chem.* **1971**, *46*, 31.
- (23) Frisch, J. M.; Trucks, G. W.; Head-Gordon, M.; Gill, P. M.; Wong, M. W.; Foresman, J. B.; Johnson, B. G.; Schlegel, H. B.; Robb, M. A.; Replogle, E. S.; Gomperts, R.; Andres, J. L.; Rachavachari, K.; Binkley, J. S.; Gonzalez, C.; Martin, R. L.; Fox, D. J.; Defrees, D. J.; Baker, J.; Stewart, J. J.; Pople, J. A. *GAUSSIAN 92*; Gaussian, Inc.: Pittsburgh, PA, 1992.
- (24) Kvisle, S.; Rytter, E. *Spectrochim. Acta* **1984**, *40A*, 939. Kvisle, S.; Rytter, E. *J. Mol. Struct.* **1984**, *117*, 51.
- (25) Collins, A. T.; Lightowlers, E. C.; Dean, P. *J. Phys. Rev.* **1967**, *158*, 3, 833.
- (26) Mazur, U., *Langmuir* **1990**, *6*, 1331.
- (27) Sipachev, V. A.; Grigor'ev, A. I. *Russ. J. Inorg. Chem.* **1970**, *15*, 905.